Complex material flow problems: a multi-scale model hierarchy and particle methods

S. Göttlich*, A. Klar†‡, S. Tiwari‡

November 19, 2014

Abstract

Material flow simulation is in increasing need of multi-scale models. On the one hand, macroscopic flow models are used for large scale simulations with a large number of parts. On the other hand microscopic models are needed to describe the details of the production process. In this paper we present a hierarchy of models for material flow problems ranging from detailed microscopic, Discrete Element Method (DEM) type, models to macroscopic models using scalar conservation laws with nonlocal interaction terms. Numerical simulations are presented on all levels of the hierarchy and the results are compared to each other for several test cases.

Keywords: interacting particles, DEM material flow simulation, diffusive limits, hydrodynamic limits, mean field equations

1 Introduction

Multi-scale models are needed for the simulation of material flow problems in large scale plant simulation, see e.g. [1]. Models on the macroscopic, as well as the microscopic and intermediate level of description are in use to describe such problems [2, 3]. In the present work we present a hierarchy of models ranging from detailed microscopic models of Newton-dynamics type to macroscopic models based on (systems of) conservation laws. Each level of the hierarchy is, at least on a formal level, derived from the underlying one.

Methods to deal with problems involving material flow or granular flow of materials have been developed on different levels of description by many authors. On the microscopic level methods, so called Discrete Element Methods (DEM), based on system of ordinary differential equations are widely used, see

*University of Mannheim, Department of Mathematics, 68131 Mannheim, Germany (goettlich@uni-mannheim.de).

†Fraunhofer Institute ITWM, Fraunhofer-Platz 1, 67663 Kaiserslautern, Germany (klar@itwm.fraunhofer.de).

‡TU Kaiserslautern, Department of Mathematics, PO Box 3049, 67653 Kaiserslautern, Germany.

for example [4, 5, 6]. On the macroscopic or hydrodynamic level methods are derived via phenomenological arguments or via kinetic theories. Examples can be found in [7, 8, 9]. From an engineering point of view, microscopic particle methods like DEM are a common tool to simulate material flow systems. However, for large systems the computational time increases rapidly with the number of particles. As an alternative, one can think of models independent of individual parts, i.e. macroscopic models.

In this work, we closely follow a procedure for interacting particle systems used, for example, in the derivation of hydrodynamic equations in swarming problems, see [10] or crowd dynamics see [11]. We derive hydrodynamic equations via a kinetic mean field limit and further scalar macroscopic approximations via simple formal arguments. The hydrodynamic equations as well as the scalar macroscopic approximations are integro-differential equations involving a non-local term. Interestingly, the scalar non-local macroscopic models also appear in crowd dynamics applications, cf. [12, 11]. Moreover, we note that similar scalar models are used in [8] for material flow simulation.

All of the above macroscopic models are finally numerically solved by a macroscopic mesh free particle method. We present different experimental setups as well as computational times.

Finally, we note that a method which is close in spirit to our numerical method, has been developed in [13, 14, 15] and is called the averaging method.

The paper is organized in the following way: in section 2 the microscopic model is presented along the lines of [6]. In section 3 the mean field and hydrodynamic limit of the microscopic system are derived. Section 4 contains the scalar limit equations for the density with nonlocal interaction or diffusion terms. In section 5 the models are applied and compared using different problems from material flow simulation.

2 The microscopic granular flow model

We consider a microscopic model for simulating material flow. In the following, we restrict our investigations for simplicity to two space dimensions, i.e., for example, a situation with a single layer of particles on a transportation belt. The model is given by a two-dimensional interacting particle system as used in Discrete Element Methods (DEM), see e.g. [6]. We note that the exact form of the microscopic system is not relevant for the following considerations. With $x_i \in \mathbb{R}^2, i = 1, \dots, N$, and velocity $v_i \in \mathbb{R}^2$ the equations of motion are

$$\frac{\mathrm{d}\mathbf{x}_i}{\mathrm{d}t} = \mathbf{v}_i, \tag{2.1a}$$

$$m\frac{\mathrm{d}\mathbf{v}_i}{\mathrm{d}t} = \sum_{i \neq j} \mathbf{F}(\mathbf{x}_i - \mathbf{x}_j, \mathbf{v}_i - \mathbf{v}_j) + \mathbf{G}(\mathbf{v}_i). \tag{2.1b}$$

Here, the bottom friction $\mathbf{G}$ is defined by

$$\mathbf{G}(\mathbf{v}) = -\mu_b mg \frac{\mathbf{v} - \mathbf{v_T}}{\|\mathbf{v} - \mathbf{v_T}\|}. \tag{2.2}$$

Here, g is the gravitational constant, m is the mass and μ_b is the bottom friction coefficient. The velocity of the belt is denoted by $\mathbf{v}_T$. Analogous to the procedure in [6] for the interaction friction forces (see below) one might introduce a regularized version of the bottom friction force

$$\mathbf{G}(\mathbf{v}) = -\min\Big(\mu_b mg,\, \gamma_b \|\mathbf{v} - \mathbf{v_T}\|\Big) \frac{\mathbf{v} - \mathbf{v_T}}{\|\mathbf{v} - \mathbf{v_T}\|}. \tag{2.3}$$

Here, γ_b is the bottom viscous damping. Moreover, using the Heaviside function H, the interaction force is given by a spring-damper model of the following form

$$\mathbf{F}(\mathbf{x}, \mathbf{v}) = H(2R - \|\mathbf{x}\|) \left(\mathbf{f^n}(\mathbf{x}, \mathbf{v}) + \mathbf{f^t}(\mathbf{x}, \mathbf{v})\right) \tag{2.4}$$

with

$$\mathbf{f^n}(\mathbf{x}, \mathbf{v}) = \mathbf{f}^n_{el}(\mathbf{x}, \mathbf{v}) + \mathbf{f}^n_{diss}(\mathbf{x}, \mathbf{v}). \tag{2.5}$$

The force $\mathbf{F}(\mathbf{x}, \mathbf{v})$ is active whenever particles collide, i.e., $2R > \|\mathbf{x}\|$, where R is the radius of the particles. Otherwise, it is inactive and the movement of particles is solely influenced by the bottom friction (2.3).

The elastic repulsive force is given by

$$\mathbf{f}^n_{el}(\mathbf{x}, \mathbf{v}) = k_n \mathbf{n}(2R - \|\mathbf{x}\|), \tag{2.6}$$

where

$$\mathbf{n} = \mathbf{n}(\mathbf{x}) = \frac{\mathbf{x}}{\|\mathbf{x}\|} \tag{2.7}$$

is the normal unit vector and k_n is the normal spring constant. The normal dissipative force is given by

$$\mathbf{f}^n_{diss}(\mathbf{x}, \mathbf{v}) = -\gamma_n \langle \mathbf{v}, \mathbf{n} \rangle \mathbf{n} \tag{2.8}$$

with γ_n the normal viscous coefficient. The tangential friction force is

$$\mathbf{f^t}(\mathbf{x}, \mathbf{v}) = -\min\left(\gamma_t \|\mathbf{v^t}\|, \mu \|\mathbf{f^n}\|\right) \frac{\mathbf{v^t}}{\|\mathbf{v^t}\|}, \tag{2.9}$$

where

$$\mathbf{v^t} = \mathbf{v} - \langle \mathbf{v}, \mathbf{n} \rangle \mathbf{n} \tag{2.10}$$

is the tangential vector pointing into the direction of the tangential component of the relative velocity. The Coulomb friction coefficient is μ and γ_t is the tangential viscous damping.

Remark 2.1 *The present paper concentrates on the modeling and simulation of material flow on a transportation belt and 2-D situations. However, the derivation of the model hierarchy as well as the particle method presented later are in no way restricted to a 2-D situation.*

3 Mean field and hydrodynamic limit

Using the so-called 'weak coupling scaling' assumption [16, 17] one rescales the interaction potential with the factor M/N where N denotes the total number of particles and M the total mass in the problem. Usually M is chosen as $M = 1$. Thus, our scaled microscopic model is given by equations (2.1) with a $1/N$ scaling of the interaction term, i.e.

$$\frac{\mathrm{d}\mathbf{x}_i}{\mathrm{d}t} = \mathbf{v}_i, \tag{3.1a}$$

$$m\frac{\mathrm{d}\mathbf{v}_i}{\mathrm{d}t} = \frac{1}{N}\sum_{i\neq j}\mathbf{F}(\mathbf{x}_i - \mathbf{x}_j, \mathbf{v}_i - \mathbf{v}_j) + \mathbf{G}(\mathbf{v}_i). \tag{3.1b}$$

Letting N tends to infinity, one can derive in the limit of a large number of particles the associated mean field equation. For the derivation we refer to [18, 10] or [11].

One obtains for the distribution function $f = f(\mathbf{x}, \mathbf{v})$ of the particles the mean field equation

$$\partial_t f + \mathbf{v}\cdot\nabla_{\mathbf{x}} f + Sf = 0 \tag{3.2}$$

with force term

$$Sf = \nabla_{\mathbf{v}}\cdot\left(\frac{1}{m}\mathbf{G}(\mathbf{v})f(\mathbf{x},\mathbf{v})\right) + \nabla_{\mathbf{v}}\cdot\left(\int\int\frac{1}{m}\mathbf{F}(\mathbf{x}-\mathbf{y},\mathbf{v}-\mathbf{w})f(\mathbf{y},\mathbf{w})\mathrm{d}\mathbf{w}\mathrm{d}\mathbf{y}f(\mathbf{x},\mathbf{v})\right). \tag{3.3}$$

For the following we define the density ρ as

$$\rho(\mathbf{x}) := \int f(\mathbf{x},\mathbf{v})\mathrm{d}\mathbf{v} \tag{3.4}$$

and the momentum by

$$\rho\mathbf{u}(\mathbf{x}) := \int \mathbf{v}f(\mathbf{x},\mathbf{v})\mathrm{d}\mathbf{v}. \tag{3.5}$$

Since the total mass M is normalized we have

$$\int \rho(\mathbf{x})\mathrm{d}\mathbf{x} = 1. \tag{3.6}$$

In the following, we derive from the mean field equation the hydrodynamic limit equations. Hydrodynamic limits for similar equations have been derived in [10, 19]. We consider the mean field equation

$$\partial_t f + \mathbf{v}\cdot\nabla_{\mathbf{x}} f + Sf = 0. \tag{3.7}$$

We integrate the kinetic equation against $\mathrm{d}\mathbf{v}$ and $\mathbf{v}\,\mathrm{d}\mathbf{v}$ and neglect fluctuations, i.e., we use a monokinetic distribution function to close the resulting equations.

The latter means that the velocity distribution function is assumed to be concentrated in the direction of the mean velocity, i.e., see for example [10]

$$f \sim \rho(\mathbf{x})\delta_{\mathbf{u}(\mathbf{x})}(\mathbf{v}). \tag{3.8}$$

This gives the continuity equation

$$\partial_t \rho + \nabla_{\mathbf{x}} \cdot (\rho \mathbf{u}) = 0 \tag{3.9}$$

and the momentum equation

$$\partial_t \mathbf{u} + \mathbf{u} \cdot \nabla_{\mathbf{x}} \mathbf{u} = \frac{1}{\rho} \int \frac{1}{m} \mathbf{G}(\mathbf{v}) f(\mathbf{x}, \mathbf{v}) \mathrm{d}\mathbf{v} \tag{3.10a}$$

$$+ \frac{1}{\rho} \int \int \int \frac{1}{m} \mathbf{F}(\mathbf{x} - \mathbf{y}, \mathbf{v} - \mathbf{w}) f(\mathbf{y}, \mathbf{w}) \mathrm{d}\mathbf{w} \mathrm{d}\mathbf{y} f(\mathbf{x}, \mathbf{v}) \mathrm{d}\mathbf{v}. \tag{3.10b}$$

Using now the monokinetic closure we obtain

$$\int \int \int \mathbf{F}(\mathbf{x} - \mathbf{y}, \mathbf{v} - \mathbf{w}) f(\mathbf{y}, \mathbf{w}) \mathrm{d}\mathbf{w} \mathrm{d}\mathbf{y} f(\mathbf{x}, \mathbf{v}) \mathrm{d}\mathbf{v} \tag{3.11a}$$

$$= \int \int \int \mathbf{F}(\mathbf{x} - \mathbf{y}, \mathbf{v} - \mathbf{w}) \rho(\mathbf{y}) \delta_{\mathbf{u}(\mathbf{y})}(\mathbf{w}) \mathrm{d}\mathbf{w} \mathrm{d}\mathbf{y} \rho(\mathbf{x}) \delta_{\mathbf{u}(\mathbf{x})}(\mathbf{v}) \mathrm{d}\mathbf{v} \tag{3.11b}$$

$$= \rho(\mathbf{x}) \int \mathbf{F}(\mathbf{x} - \mathbf{y}, \mathbf{u}(\mathbf{x}) - \mathbf{u}(\mathbf{y})) \rho(\mathbf{y}) \mathrm{d}\mathbf{y} \tag{3.11c}$$

$$=: \rho(\mathbf{x}) \mathbf{F}^\star(\rho, \mathbf{u})(\mathbf{x}) \tag{3.11d}$$

and altogether an equation for the mean velocity

$$\partial_t \mathbf{u} + (\mathbf{u} \cdot \nabla_{\mathbf{x}}) \mathbf{u} = \frac{1}{m} \mathbf{G}(\mathbf{u}) + \frac{1}{m} \mathbf{F}^\star(\rho, \mathbf{u}) \tag{3.12}$$

which is solved together with the continuity equation (3.9).

4 Scalar limit equations

Scalar limit equations for interacting particle systems have been derived, for example in [10, 20]. Rigorous results on the convergence of hydrodynamic equations with damping to the porous media equation can be found, for example in [21]. We proceed as follows. Starting from the hydrodynamic momentum equation we use a quasi-stationary approximation of the momentum equation, setting time and spatial derivatives to zero. This can be interpreted here as considering comparatively small values of the mass m. We obtain

$$\mathbf{G}(\mathbf{u}) = -\mathbf{F}^\star(\rho, \mathbf{u}) \tag{4.1}$$

with $\mathbf{G}(\mathbf{u})$ given by

$$\mathbf{G}(\mathbf{u}) = -\min\Big(\mu_b m g,\, \gamma_b \|\mathbf{u} - \mathbf{v_T}\|\Big) \frac{\mathbf{u} - \mathbf{v_T}}{\|\mathbf{u} - \mathbf{v_T}\|} \tag{4.2}$$

and

$$\mathbf{F}^\star(\rho,\mathbf{u}) = \int \mathbf{F}(\mathbf{x}-\mathbf{y},\mathbf{u}(\mathbf{x})-\mathbf{u}(\mathbf{y}))\rho(\mathbf{y})\mathrm{d}\mathbf{y}. \tag{4.3}$$

We have to determine a solution $\mathbf{u}$ of this integral equation for fixed ρ. The result is used to close the continuity equation. In the general case the existence of a solution of the equation is not obvious. However, a simplified version of the equation is easily solved. For small values of $\mathbf{u}-\mathbf{v_T}$ we have

$$\mathbf{G}(\mathbf{u}) = \gamma_b(\mathbf{v_T}-\mathbf{u}). \tag{4.4}$$

Moreover, we assume that the elastic normal force dominates the friction forces. This means $\mathbf{F}$ does not depend on $\mathbf{u}$ or $\mathbf{F}^\star(\rho,\mathbf{u}) = \mathbf{F}\star\rho$. Then, we have to solve

$$\gamma_b(\mathbf{v_T}-\mathbf{u}) = -\mathbf{F}\star\rho \tag{4.5}$$

or

$$\mathbf{u} = \mathbf{v_T} + \frac{1}{\gamma_b}\mathbf{F}\star\rho. \tag{4.6}$$

The resulting scalar equation is then

$$\partial_t\rho + \nabla_\mathbf{x}\cdot(\mathbf{v_T}\rho) + \nabla_\mathbf{x}\cdot\Big(\frac{1}{\gamma_b}(\mathbf{F}\star\rho)\rho\Big) = 0. \tag{4.7}$$

Remark 4.1 *One might derive an associated diffusive equation as well, compare [20], for the more complicated case of swarming models. To do so, we write the force* $\mathbf{F}$ *as a gradient field with* $\mathbf{F} = -\nabla U$*. Using the above simplifications we have* $\mathbf{F}(\mathbf{x}) = k_n(\mathbf{x})(2R-\|\mathbf{x}\|)$ *for* $\|\mathbf{x}\| < 2R$ *and*

$$U = k_n\left(2R^2 - \|\mathbf{x}\|(2R - \frac{\|\mathbf{x}\|}{2})\right) \tag{4.8}$$

for $\|\mathbf{x}\| < 2R$*. Approximating the potential* U *by a* δ *distribution, i.e.*

$$U(\mathbf{y}) \sim D\delta_\mathbf{0}(\mathbf{y}) \tag{4.9}$$

with the constant $D > 0$ *given by*

$$D = \int U(\mathbf{y})\mathrm{d}\mathbf{y} \tag{4.10}$$

and using the symmetry of the convolution

$$\int \nabla_\mathbf{x}U(\mathbf{x}-\mathbf{y})\rho(\mathbf{y})\mathrm{d}\mathbf{y} = -\int \nabla_\mathbf{y}U(\mathbf{x}-\mathbf{y})\rho(\mathbf{y})\mathrm{d}\mathbf{y} = \int U(\mathbf{x}-\mathbf{y})\nabla_\mathbf{y}\rho\mathrm{d}\mathbf{y} \tag{4.11}$$

and

$$\mathbf{F}\star\rho = -\int U(\mathbf{x}-\mathbf{y})\nabla_\mathbf{y}\rho\mathrm{d}\mathbf{y} \sim -D\nabla_\mathbf{x}\rho \tag{4.12}$$

we obtain the following equation

$$\partial_t \rho + \nabla_{\mathbf{x}} \cdot (\mathbf{v_T} \rho) = D \nabla_{\mathbf{x}} \cdot \Big(\frac{1}{\gamma_b} \rho \nabla_{\mathbf{x}} \rho \Big). \tag{4.13}$$

Thus, this procedure reduces the problem to a porous media equation with drift term.

Remark 4.2 *We note that (4.7) is similar to an equation considered in [12] for modeling pedestrian crowds and used in [8] for material flow simulation. There, equations of the form*

$$\partial_t \rho + \nabla_{\mathbf{x}} \cdot (\mathbf{v_T} \rho) + \nabla_{\mathbf{x}} \cdot \left(\frac{\nabla_{\mathbf{x}} (\eta \star \rho)}{\sqrt{1 + \|\nabla_{\mathbf{x}} (\eta \star \rho)\|^2}} \rho \right) = 0 \tag{4.14}$$

have been considered. This is equivalent to (4.7) if $-\eta$ is identified with the potential U, where $-\nabla_{\mathbf{x}} U = \mathbf{F}$ and

$$\frac{1}{\gamma_b} = \frac{1}{\sqrt{1 + \|\nabla_{\mathbf{x}} (\eta \star \rho)\|^2}}. \tag{4.15}$$

5 Numerical investigations

In this section we present a series of numerical experiments on the microscopic equations (3.1), as well as the hydrodynamic and scalar limit equations (3.9),(3.12) and (4.7). Different situations are studied and various patterns are investigated. In general, we observe the following: For a large number of particles microscopic and hydrodynamic equations yield similar results in all cases studied here. The scalar limit equation deviates from these solutions in certain cases. Qualitatively they still give similar results. This deviation is, in the examples and for the parameters considered here, essentially due to using the quasi-stationary approximation of the momentum equation described above in the derivation of the scalar limit equation. Using (2.3) instead of (4.4) and neglecting the friction forces $\mathbf{f}^n_{diss}$ and $\mathbf{f}^t$ in the hydrodynamic simulation does not change the results significantly for the parameters considered in the following. From the point of view of computation time all equations require approximately the same amount of time per particle used in the simulations. The advantage of using the macroscopic limit equations lies in the fact that, in particular, for situations with a large number of microscopic particles the number of macroscopic particles can be strongly reduced obtaining still very similar results.

5.1 Numerical methods

The microscopic equations are solved using a simple explicit Euler scheme for systems of ordinary differential equations. For a straightforward implementation, the complete distance matrix $(d_{i,j}) = |\mathbf{x}_i - \mathbf{x}_j|$ has to be computed in order to evaluate the interaction potential. Since this is costly, there is a restriction

on the number of particles which can be simulated in this way. A more sophisticated implementation uses nearest neighbor lists. In the present microscopic simulations as well as in the particle method for the hydrodynamic equations an implementation based on a nearest neighbor list is used.

The hydrodynamic limit equations (3.9),(3.12) are considered in detail numerically using a macroscopic particle method, see [22]. The particle method is based on a Lagrangian formulation of the hydrodynamic equations (3.9),(3.12):

$$\frac{\mathrm{d}\mathbf{x}}{\mathrm{d}t} = \mathbf{u}, \tag{5.1a}$$

$$\frac{\mathrm{d}\rho}{\mathrm{d}t} = -\rho\nabla_{\mathbf{x}} \cdot \mathbf{u}, \tag{5.1b}$$

$$\frac{\mathrm{d}\mathbf{u}}{\mathrm{d}t} = \frac{1}{m}\mathbf{G}(\mathbf{u}) + \frac{1}{m}\mathbf{F}^{\star}(\rho, \mathbf{u}), \tag{5.1c}$$

where $\mathrm{d}/\mathrm{d}t = \partial_t + \mathbf{u}\cdot\nabla_{\mathbf{x}}$. Quantities, like, for example, the derivatives, appearing on the right hand side are approximated at the particle location $\mathbf{x}$ from the surrounding neighbor particles at $\mathbf{x}_j$ using weight functions. In order to restrict the number of neighboring point we associate a weight function $w = w(\mathbf{x}_j - \mathbf{x}, h)$ with small compact support of size h. In the present computation we use a Gaussian weight function in the following form

$$w(\mathbf{x}_j - \mathbf{x}, h) = \begin{cases} \exp(-\alpha \frac{\|\mathbf{x}_i - \mathbf{x}\|^2}{h^2}), & \text{if } \frac{\|\mathbf{x}_j - \mathbf{x}\|}{h} \leq 1, \\ 0, & \text{else}, \end{cases} \tag{5.2}$$

where α is a positive constant and is considered to be equal to 6.25. The radius h is approximately chosen 4 times the particle radius to include enough particles for a stable approximation of the equations, see [22] for details. We note that smoothing functions are also used in the averaging methods [15] mentioned in the introduction. The integral over the interaction potential is in most cases evaluated by a straightforward integration rule:

$$\mathbf{F}^{\star}(\rho, \mathbf{u}) \sim \sum_j \mathbf{F}(\mathbf{x} - \mathbf{x}_j, \mathbf{u}(\mathbf{x}) - \mathbf{u}_j)\rho_j \mathrm{d}\mathbf{V}_j, \tag{5.3}$$

where $\mathrm{d}\mathbf{V}_j$ is the local area around a particle determined by a nearest neighbor search. In case the numerical simulation is underresolved a higher order approximation of the integral has to be implemented. We refer to [23] for details. The resulting system of ordinary differential equations is then solved again by a first order time discretization method. Diffusive terms can be included as well in a straightforward way. Obviously, this shows that the actual macroscopic computations are very similar to the microscopic ones. A major difference is the procedure to evaluate the interaction term. In the microscopic case we compute

$$\frac{1}{N}\sum_j \mathbf{F}(\mathbf{x} - \mathbf{x}_j, \mathbf{v} - \mathbf{v}_j) \tag{5.4}$$

instead of the above expression. If the values of ρ_j and $\mathrm{d}\mathbf{V}_j$ are all equal then using

$$1 = \int \rho(\mathbf{x})\mathrm{d}\mathbf{x} \sim \sum_j \rho_j \mathrm{d}\mathbf{V}_j \tag{5.5}$$

it is easy to see that $\rho_j \mathrm{d}\mathbf{V}_j = 1/N$ and both terms (5.3) and (5.4) are equal. However, in the macroscopic situation the particles are not physical particles as in the microscopic case. They play the role of discretization points. In particular, if the number of 'real' particles is very large, that does not mean that the number of macroscopic particles in the particle method has to be increased in the same way. The number of macroscopic particles is only chosen according to accuracy considerations. On the other hand, the macroscopic equations considered here are derived under the assumption of a monokinetic distribution function. Thus, they are not able to capture all microscopic patterns, compare, for example, the appearance of double mills in microscopic swarming simulations, see [10].

Finally, the scalar equation is solved as well with a particle method. In this case the so called diffusion velocity methods, see [24], are used. This means, equation (4.7) is written as a pure transport problem

$$\partial_t \rho + \nabla_{\mathbf{x}} \cdot (\mathbf{u}\rho) = 0 \tag{5.6}$$

with

$$\mathbf{u} = \mathbf{v_T} + \frac{1}{\gamma_b}\mathbf{F} \star \rho \tag{5.7}$$

and then solved in a Lagrangian way. The approximation of the convolution term is done as for the hydrodynamic models. Boundary conditions are realized by using fixed boundary particles with a suitable interaction potential.

5.2 Numerical comparison of the microscopic, hydrodynamic and diffusive equations

In this section we investigate different configurations for material flow in 2-D ranging from a simple diffusion problem to modeling material on a conveyor belt with slides and junctions. For the following comparisons we consider the microscopic solution as the reference solution and compare the hydrodynamic and scalar approximation with the microscopic solution. The first example treats diffusion of particles, compare also [23]. Examples 2, 3 and 4 describe test cases relevant for material flow problems.

5.2.1 Example 1 (Diffusion):

This example studies the diffusion of the density without motion of the belt and boundary conditions. It has been partially discussed in [23]. In this situation particles are artificially compressed in a region in the center of the domain. As time proceeds the support of the density becomes larger and larger, compare the Barenblatt solution of the porous media equation [25]. For the microscopic

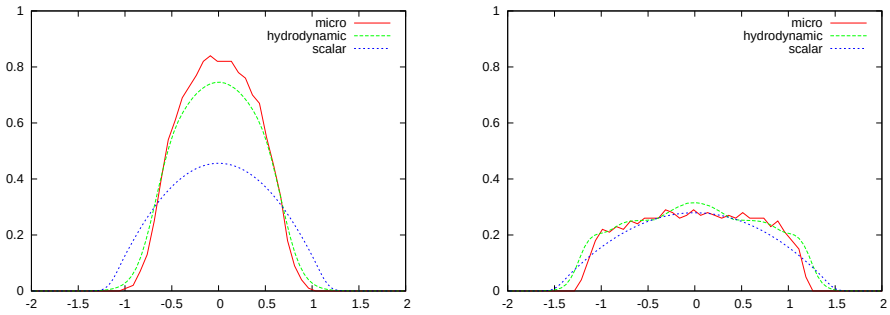

(a) $t = 0.2$ (b) $t = 0.6$

Figure 1: Comparison of the density determined from microscopic, hydrodynamic and scalar model for short and long times.

model this terminates if the compact support of the interaction kernels of the finite number of particles do not overlap any more.

We consider a 2-D situation, a friction force

$$\mathbf{G}(\mathbf{v}) = -\mathbf{v}, \tag{5.8}$$

that means we choose $\mathbf{v_T} = 0$, $\mu_b = \infty$, $\gamma_b = 1$. Moreover, we choose $m = 1$, where N is the initial number of particles and $R = 0.0375$, $k_n = 3/(2R^4\pi)$ such that $D = 2$. Intermolecular friction is neglected, i.e. $\gamma_n = \mu = \gamma_t = 0$. We use 17 383 particles for the microscopic and 6 400 particles representing the 'grid' for the macroscopic model. In Figure 1 the densities determined from the microscopic, the hydrodynamic and the scalar approximation are compared to each other for short and long time $t = 0.2, 0.6$.

One observes in Figure 1(b) that all solutions have a similar long time behavior, compare [21]. For shorter times hydrodynamic and microscopic solutions still show a similar behavior, whereas the scalar solution is at least qualitatively correct (for example, the speed of propagation) but shows quantitative deviations (stronger diffusivity). This is quantified in Figure 2, where the distance (in the L^2-norm) between the hydrodynamic and scalar solution is shown versus time.

The difference in approximation quality between hydrodynamic and scalar approximation is clearly observed. This could be rephrased in terms of the assumptions leading to the different approximations. In the present simulations, the assumptions leading to the hydrodynamic approximation (chaos assumption and monokinetic closure) are obviously more justified for the present set of parameters than neglecting the inertia terms, which finally leads to the scalar approximation. This is due to the fact that $D = \int U(\mathbf{y})\mathrm{d}\mathbf{y} = 2$ and $\gamma_b = 1$. In this case the scalar approximation is still far from the hydrodynamic solution. If D and γ_b would be chosen large, we would observe that microscopic, hydrodynamic and scalar models yield very similar solutions.

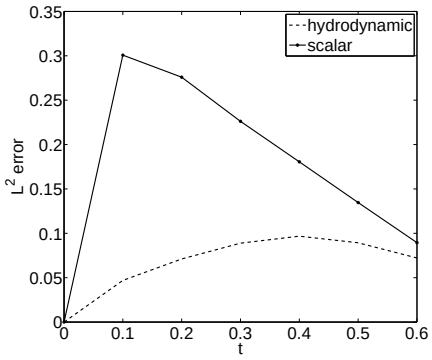

Figure 2: Comparison of the L^2-error between hydrodynamic (dotted line) and scalar model (straight line).

Remark 5.1 *Finally, we remark that a comparison of the computation times for microscopic, hydrodynamic and scalar models for the present example can be found in [23]. This comparison clearly shows the advantage of using macroscopic particle methods compared to microscopic simulations. In particular, computation time is strongly reduced using the macroscopic method, if the number of real microscopic particles in a system is large.*

5.2.2 Example 2 (Slider):

This and the following examples are used to compare the time evolution for the different models in a situation where diffusion is small compared to the advection given by the belt motion. The second test example shows the time evolution in a channel flow with a slider. We choose the parameter $m = 1/N$, $R = 0.375$, $\mathbf{v_T} = (2, 0)$, $\mu_b = 200 \times m, \mu = 2 \times m, \gamma_t = 2 \times m$. Additionally, we set here $\gamma_b = 60$, $k_n = 2 \times 10^7 \times m$ and $\gamma_n = 4 \times 10^6 \times m$. First we consider a situation with a fixed number of microscopic particles entering the domain from the left and being transported on the conveyor belt to the right. For this comparison we use $N = 246$ microscopic particles and the same number of 'grid'-particles for the macroscopic solution Figure 3 shows the time evolution of the particles for the microscopic, macroscopic and scalar model for times $t = 1.125, 1.5, 2.0$. Quantitatively all three solutions have a similar behavior. Qualitatively, the hydrodynamic solution shows a slightly closer agreement with the microscopic one as the scalar solution. The computations times for the three models are similar in this case, since the number of particles used are equal. Figure 4 shows the amount of cargo that passes the slider. The solutions show the relative number of particles in the region in front of the obstacle at $x = 4$. The hydrodynamic solution captures the time decay of the microscopic outflow nearly exactly, see Figure 4. In particular, it is a better approximation of the time dependent microscopic outflow than the outflow determined from

the scalar equation.

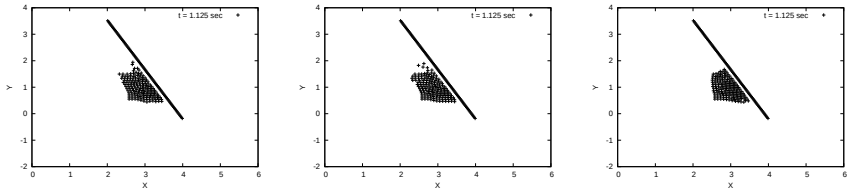

(a) Microscopic, t=1.125 (b) Hydrodynamic,t=1.125 (c) Scalar, t=1.125

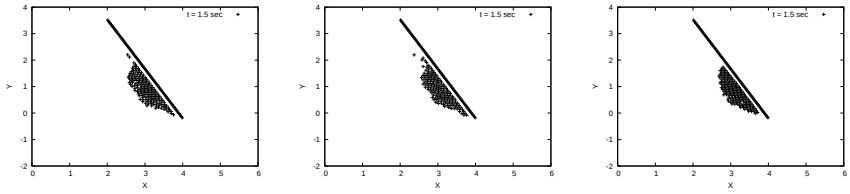

(d) Microscopic, t=1.5 (e) Hydrodynamic, t=1.5 (f) Scalar, t=1.5

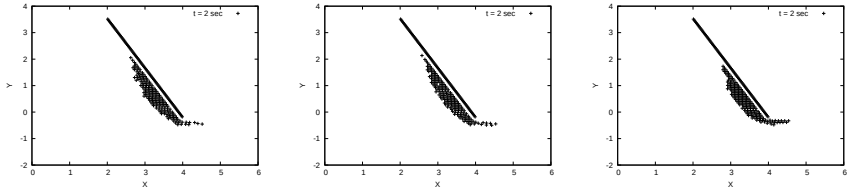

(g) Microscopic, t=2.0 (h) Hydrodynamic, t=2.0 (i) Scalar, t=2.0

Figure 3: Distribution of particles for microscopic, hydrodynamic and scalar models at different times.

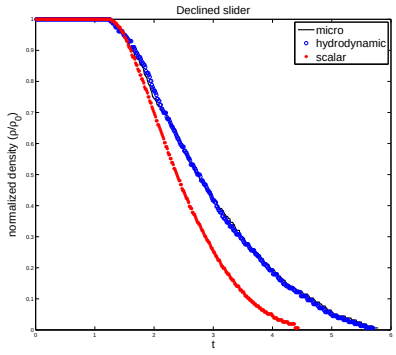

Figure 4: Comparison of the outflow. We measure the normalized number of parts at $x = 4$.

5.2.3 Example 3 (Slider with constant inflow):

Next we consider a constant stream of ingoing particles. We use this example to compare the solutions of the scalar and hydrodynamic model in more detail. The following figures show the distribution of particles for a long time t until a stationary state is obtained. Figure 5 shows the densities for hydrodynamic and scalar model.

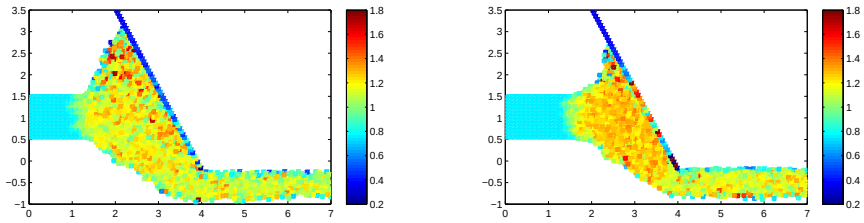

(a) Hydrodynamic (b) Scalar

Figure 5: Density for hydrodynamic and scalar models at large time for constant stream of particles.

Figure 6 shows the velocities for hydrodynamic and scalar model.

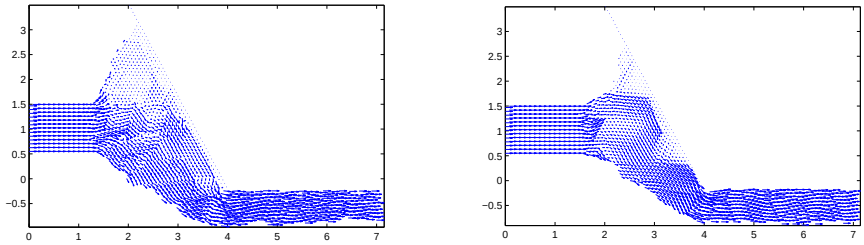

(a) Hydrodynamic (b) Scalar

Figure 6: Velocity field for hydrodynamic and scalar models at large time for constant stream of particles.

Figure 7 shows the densities and velocities in x-direction for hydrodynamic and scalar model for the above computation along a cut at $y = 1$.

For all quantities one observes a good coincidence between scalar and hydrodynamic model for the present situation.

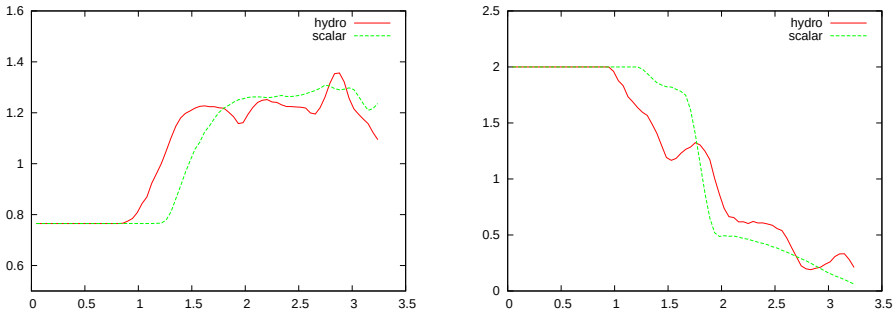

(a) Density (b) Velocity

Figure 7: Density and velocity in x-direction for hydrodynamic and scalar models at large time for constant stream of particles at $y = 1$.

5.2.4 Example 4 (Orthogonal slider):

The same situation as in Example 2 is shown in Figure 8 with an orthogonal slider. Only the solution of the hydrodynamic model is presented. The figures show that most of the particles pass through the channel. A small part of the particles, however, is trapped by the orthogonal slider.

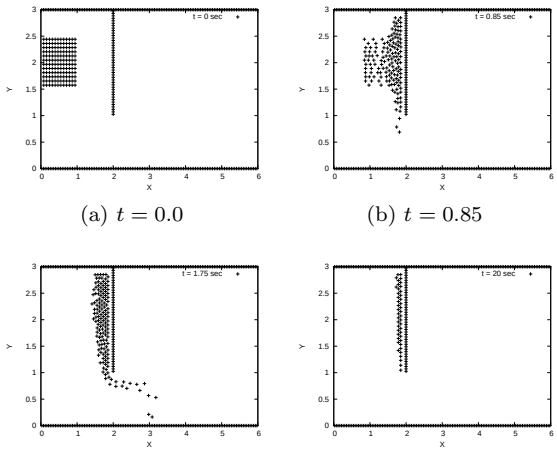

(a) $t = 0.0$ (b) $t = 0.85$

(c) $t = 1.75$ (d) $t = 20.0$

Figure 8: Distribution of particles for hydrodynamic models $t = 0, 0.85, 1.75$ and $t = 20.0$ for orthogonal slider.

A comparison of the outflow is given as for the previous example in Figure 9. Again there is a good coincidence between hydrodynamic and microscopic model. Only the final number of trapped particles differs slightly.

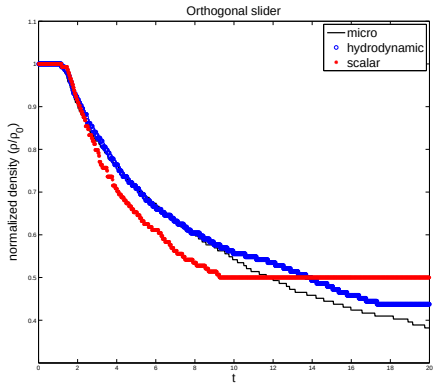

Figure 9: Comparison of the outflow. We measure the normalized number of parts at $x = 2$.

5.2.5 Example 5 (Junction):

Finally,we consider a junction modeled by a conveyor belt from left to right with an ingoing belt from below. The belt speeds are orthogonal to each other. The parameters are chosen as above. Again the hydrodynamic model is shown. The comparison for the particles is shown in Figure 10.

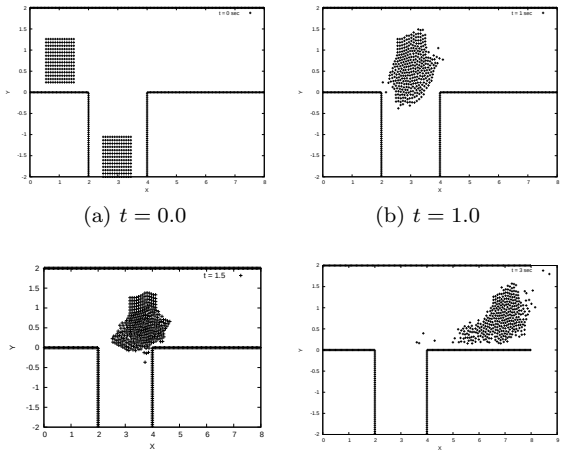

(a) $t = 0.0$ (b) $t = 1.0$

(c) $t = 1.5$ (d) $t = 3.0$

Figure 10: Distribution of particles for hydrodynamic models $t = 0.0, 1.0, 1.5$ and $t = 3.0$ for a junction.

We observe a collision of the bulk of particles in the junction. This results in a merger of the bulks and a small part of particles dragged behind the bulk part.

A comparison of the outflow is given as for the previous examples in Figure 11. There is a perfect fit between hydrodynamic and microscopic solution, whereas the simpler scalar model gives a solution which deviates slightly from the microscopic one.

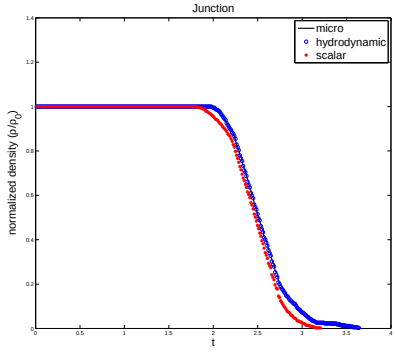

Figure 11: Comparison of the outflow. We measure the normalized number of parts before a vertical line at $x = 6$.

6 Concluding Remarks

We have presented a numerical discussion of a model hierarchy for material or granular flow simulations. All models show a quantitatively correct behavior. The advantage of considering a system of equations for density and momentum, i.e. a hydrodynamic approximation, compared to a scalar (nonlocal) conservation law is clearly observed for certain parameter values. Lagrangian particle methods are a natural choice for the above problems. Further research will concentrate on applying the above methods to more complex and large scale material flow problems like, for example, particles of different size or mass or three dimensional problems with more complex geometry.

Acknowledgment

This work is supported by the German research foundation, DFG grants KL 1105/20-1, GO 1920/3-1 and the BMBF Project KinOpt.

References

[1] S. Hoher, P. Schindler, S. Göttlich, V. Schleper, S. Röck, *System Dynamic Models and Real-time Simulation of Complex Material Flow Systems*. In: H. A. ElMaraghy, Enabling Manufacturing competitiveness and economic sustainability 2012, Part 3 (2011) 316-321.

[2] M. Jahangirian, T. Eldabi, A. Naseer, L.K. Stergioulas, T. Young, *Simulation in manufacturing and business: A review*. European J. Oper. Res. 203 (2012) 1-13.

[3] G. Reinhart, F. Lacour, *Physically based Virtual Commissioning of Material Flow Intensive Manufacturing Plants*. In: Zaeh, M. F.; ElMaraghy, H. A.: 3rd International Conference on Changeable, Agile, Reconfigurable and Virtual Production (CARV 2009) 377-387.

[4] P.W. Cleary, M.L. Sawley, *DEM modeling of industrial granular flows: 3D case studies and the effect of particle shape on hopper discharge*. Appl. Math. Model. 26 (2002) 89-111.

[5] P.A. Cundall, O.D.L. Strack, *A discrete numerical model for granular assemblies*. Geotechnique 29 (1979) 47-65.

[6] M. Lätzel, S. Luding, H.J. Hermann, *Macroscopic material properties from quasi-static, microscopic simulations of a two-dimensional shear-cell*. Granular Matter 2 (2000) 123-135.

[7] C.S. Campbell, *Rapid granular flows*. Annu. Rev. Fluid Mech. 22 (1990) 57-92.

[8] S. Göttlich, S. Hoher, P. Schindler, V. Schleper, A. Verl, *Modeling, simulation and validation of material flow on conveyor belt*. Appl. Math. Model. 38 (2014) 3295-3313.

[9] C.K.K. Lun, S.B. Savage, D.J. Jeffrey, N. Chepurniy, *Kinetic theories for granular flow: inelastic particles in Couette flow and slightly inelastic particles in a general flowfield*. J. Fluid Mech. 140 (1984) 223-256.

[10] J.A. Carrillo, M.R. D'Orsogna, V. Panferov, *Double milling in self-propelled swarms from kinetic theory*. Kinet. Relat. Models 2 (2009) 363-378.

[11] R. Etikyala, S. Göttlich, A. Klar, S. Tiwari, *Particle methods for pedestrian flow models: from microscopic to non-local continuum models*. Math. Models Methods Appl. Sci. 24 (2014), 2503-2523.

[12] R. Colombo, M. Garavello, M. Lecureux-Mercier, *A Class of Non-Local Models for Pedestrian Traffic*. Math. Models Methods Appl. Sci. 22 (2012) 1150023.

[13] M. Babic, *Average balance equations for granular materials*. Int. J. Eng. Sci. 35 (1997) 523-548.

[14] H.P. Zhu, A.B. Yu, *Averaging method of granular materials*. Phys. Rev. E 66 (2002) 021302.

[15] H.P. Zhu, A.B. Yu, *Micromechanic modeling and analysis of unsteady-state granular flow in a cylindrical hopper*. J. Engrg. Math. 52 (2005) 307-320.

[16] W. Braun, K. Hepp, *The Vlasov Dynamics and Its Fluctuations in the 1/N Limit of Interacting Classical Particles*. Commun. Math. Phys. 56 (1977) 101-113.

[17] H. Neunzert, *The Vlasov equation as a limit of Hamiltonian classical mechanical systems of interacting particles*. Trans. Fluid Dynamics 18 (1977) 663-678.

[18] J.A. Cañizo, J.A. Carrillo, J. Rosado, *A well-posedness theory in measures for some kinetic models of collective motion*. Math. Models Methods Appl. Sci. 21 (2011) 515-539.

[19] Y.L. Chuang, M.R. D'Orsogna, D. Marthaler, A.L. Bertozzi, L. Chayes, *State transitions and the continuum limit for a 2D interacting, self-propelled particle system*. Physica D 232 (2007) 33-47.

[20] C.M. Topaz, A.L. Bertozzi, *Swarming patterns in a two-dimensional kinematic model for biological groups*. SIAM J. Appl. Math. 65 (2004) 152-174.

[21] F. Huang, P. Marcati and R. Pan, *Convergence to the Barenblatt Solution for the Compressible Euler Equations with Damping and Vacuum*. Arch. Rational Mech. Anal. 176 (2005) 1-24.

[22] S. Tiwari, J. Kuhnert, *Modelling of two-phase flow with surface tension by Finite Point-set method (FPM)*. J. Comp. Appl. Math. 203 (2007) 376-386.

[23] A. Klar, S. Tiwari, *A multi-scale meshfree particle method for macroscopic mean field interacting particle models*. Multiscale Model. Simul. 12 (2014) 11671192.

[24] P. Degond, F.J. Mustieles, *Approximation of diffusion equations by deterministic convections of particles*. SIAM J. Sci. Statist. Comput. (1990) 293-310.

[25] D.G. Aronson, *Regularity properties of flows through porous media*. SIAM J. Appl. Math., 17 (1969) 461-467.